

Evaluation of cortical plasticity in children with cerebral palsy undergoing constraint-induced movement therapy based on functional near-infrared spectroscopy

Jianwei Cao
Bilal Khan
Nathan Hervey
Fenghua Tian
Mauricio R. Delgado
Nancy J. Clegg
Linsley Smith
Heather Roberts
Kirsten Tulchin-Francis
Angela Shierk
Laura Shagman
Duncan MacFarlane
Hanli Liu
George Alexandrakis

Evaluation of cortical plasticity in children with cerebral palsy undergoing constraint-induced movement therapy based on functional near-infrared spectroscopy

Jianwei Cao,^a Bilal Khan,^a Nathan Hervey,^a Fenghua Tian,^a Mauricio R. Delgado,^{b,d} Nancy J. Clegg,^b Linsley Smith,^b Heather Roberts,^b Kirsten Tulchin-Francis,^b Angela Shierk,^b Laura Shagman,^c Duncan MacFarlane,^c Hanli Liu,^a and George Alexandrakis^{a,*}

^aUniversity of Texas at Arlington and University of Texas Southwestern Medical Center at Dallas, Joint Graduate Program in Biomedical Engineering, Arlington, Texas 76010, United States

^bTexas Scottish Rite Hospital for Children, Department of Neurology, Dallas, Texas 75219, United States

^cUniversity of Texas at Dallas, Department of Electrical Engineering, Richardson, Texas 75080, United States

^dUniversity of Texas Southwestern Medical Center at Dallas, Department of Neurology, Dallas, Texas 75235, United States

Abstract. Sensorimotor cortex plasticity induced by constraint-induced movement therapy (CIMT) in six children (10.2 ± 2.1 years old) with hemiplegic cerebral palsy was assessed by functional near-infrared spectroscopy (fNIRS). The activation laterality index and time-to-peak/duration during a finger-tapping task and the resting-state functional connectivity were quantified before, immediately after, and 6 months after CIMT. These fNIRS-based metrics were used to help explain changes in clinical scores of manual performance obtained concurrently with imaging time points. Five age-matched healthy children (9.8 ± 1.3 years old) were also imaged to provide comparative activation metrics for normal controls. Interestingly, the activation time-to-peak/duration for all sensorimotor centers displayed significant normalization immediately after CIMT that persisted 6 months later. In contrast to this improved localized activation response, the laterality index and resting-state connectivity metrics that depended on communication between sensorimotor centers improved immediately after CIMT, but relapsed 6 months later. In addition, for the subjects measured in this work, there was either a trade-off between improving unimanual versus bimanual performance when sensorimotor activation patterns normalized after CIMT, or an improvement occurred in both unimanual and bimanual performance but at the cost of very abnormal plastic changes in sensorimotor activity. © The Authors. Published by SPIE under a Creative Commons Attribution 3.0 Unported License. Distribution or reproduction of this work in whole or in part requires full attribution of the original publication, including its DOI. [DOI: [10.1117/1.JBO.20.4.046009](https://doi.org/10.1117/1.JBO.20.4.046009)]

Keywords: functional near-infrared spectroscopy; cerebral palsy; constraint-induced movement therapy; sensorimotor cortex; resting-state functional connectivity.

Paper 140724RR received Nov. 3, 2014; accepted for publication Mar. 30, 2015; published online Apr. 21, 2015.

1 Introduction

Cerebral palsy (CP) describes a group of permanent neurodevelopmental disorders, the core feature of which is abnormal gross and fine motor function caused by a nonprogressive lesion to the brain that occurred in the developing fetal or infant brain.¹⁻³ Hemiplegic cerebral palsy is one of the most prevalent types of CP, characterized by unilateral motor and/or sensory impairments in the upper and lower limbs. Patients with hemiplegic CP often help their affected limb while performing daily tasks by compensatory use of their unaffected limb.^{4,5} Even though CP cannot be cured, motor control skills in these children can be improved through repetitive task-specific treatments targeting an increased involvement of the affected limb.⁶ Constraint-induced movement therapy (CIMT) is one such common treatment for children with upper limb hemiplegia.⁷ The aim of CIMT is to restrain the unaffected extremity, and thus forces intensive use of the affected extremity.⁸

Upper limb motor severity in patients with CP can be classified using the manual ability classification system (MACS).⁹ Several upper extremity functional outcome measures have been developed and validated in this population.^{10,11} The Melbourne assessment¹² measures unilateral upper limb function, while assisting hand assessment (AHA)¹³ measures bimanual function. Although very useful, clinical assessments do not yield insights about how improved motor performance relates to therapy-induced plastic changes in the brain, for which functional imaging methods are needed.^{14,15}

Functional magnetic resonance imaging (fMRI) is the gold standard for neuroimaging employed in a few recent studies to evaluate the effects of CIMT on children with CP.¹⁶⁻¹⁸ In these studies, the laterality index of sensorimotor activation between the two cerebral hemispheres^{16,18} was proposed as a measure of treatment response. However, fMRI requires subjects to remain steady for long periods of time in a restricted space, which limits the success rate of functional imaging studies in healthy children.¹⁹ This may be even more relevant in children with CP. Changes in gray matter volume in the sensorimotor cortex of the lesioned hemisphere measured by

*Address all correspondence to: George Alexandrakis, E-mail: galex@uta.edu

anatomical MRI were also proposed as a treatment response metric,¹⁷ though this approach does not offer measures of change in brain function. In addition, changes in motor-evoked potentials of the affected hand were quantified by transcranial magnetic stimulation as an alternative treatment response metric.²⁰

In recent years, fNIRS has been increasingly shown as a viable alternative neuroimaging modality to fMRI for monitoring brain activation.^{21,22} FNIRS detects changes in near-infrared light absorption caused by changes in the concentration of oxyhemoglobin (ΔHbO) and deoxyhemoglobin (ΔHb) resulting from neuronal activity, known as neurovascular coupling.²³ As light penetration in the brain is limited due to multiple scattering, fNIRS can only image cortical regions with limited spatial resolution.^{24,25} However, the portability and relative robustness of this technology to motion artifacts^{26–28} make it advantageous for monitoring brain activity in children with motor deficits, as is the case for CP. Several studies utilized fNIRS to investigate cortical activation in response to motor skills in individuals with CP.^{29–31} We have previously demonstrated that fNIRS can be used to image sensorimotor cortex activity in children with CP and derived a variety of related activation metrics.³¹ However, no fNIRS studies have been performed to date that use activation metrics for assessing plasticity in children with CP after CIMT and any related information reported in fMRI studies so far remains very limited.^{16–18}

In this work, we demonstrate how analysis of sensorimotor cortex activation patterns obtained by fNIRS during finger tapping enables quantification of spatial and temporal activation metrics for assessing plastic changes, immediately after, and 6 months after CIMT. Changes in resting-state functional connectivity patterns between sensorimotor centers are also explored as an additional metric for assessing treatment effects. Furthermore, changes in manual performance were quantified using the Melbourne and AHA clinical scales at the same time points as fNIRS measurements. The observed differences in trends between fNIRS-based metrics relative to clinical metrics provide insights into how cortical plasticity can affect manual performance. The findings of this work are a first step toward future exploration of the intriguing possibility of using fNIRS-based metrics as long-term predictors of CIMT outcomes.

2 Methods

2.1 Subjects and CIMT

Six subjects with hemiplegic CP (two female and four male; 10.2 ± 2.1 years old) were included in this study. Two subjects (Subject 4 and Subject 8) were right hemiparetic and the other four subjects were left hemiparetic. Two subjects (Subject 1 and Subject 4) were classified as MACS 1 and the other four subjects (Subject 3, 6, 7, and 8) as MACS 2. Subjects with light impairment of their affected hand that was often hardly noticeable were classified as MACS 1. Subjects classified as MACS 2 had impaired use of their affected hand, but could perform life daily activities adequately through compensatory use of their unaffected hand. Five healthy children (two female and three male; 9.8 ± 1.3 years old) were also included as controls. All the controls were right handed. All children with CP included in this study had a successful MRI scan that identified a single subcortical/cortical lesion affecting their motor area in one of the two cerebral hemispheres. In addition, Subject 3 had undergone

a right functional peri-insular hemispherectomy due to intractable epileptic seizures and had a physical shift of 1.3 cm to the right of the brain midline separating the two hemispheres, as verified by the anatomical MRI. The children with CP participated in a 2-week, pirate themed, CIMT camp that took place 5 days a week, 6 h a day, at the Texas Scottish Rite Hospital for Children in Dallas. During CIMT camp, the children took part in group and individual activities such as ball games and painting, focused on improving gross and fine motor skills and increasing independence with activities of daily living under the supervision of occupational therapists. The unaffected arm of each child was immobilized by a removable splint during camp hours, which forced the use of their affected arm during play activities. FNIRS measurements, MACS⁹ classification, and clinical assessments using the Melbourne assessment of upper limb function,¹² and AHA¹³ of bimanual limb function were performed on each child with CP before, immediately after, and 6 months after therapy. Only Subject 4 missed one fNIRS measurement at 6 months after therapy. The occupational therapists inquired about the children's affected arm activity levels after therapy and although these varied between subjects no additional therapies or intensive manual training were performed by any subject in the 6 months after CIMT. Control subjects were also measured by fNIRS at the same time points, but no clinical assessments were performed on them. The study was approved by the University of Texas Southwestern Medical Center at Dallas (UTSW) Institutional Review Board protocol (IRB No. 042007-064).

2.2 Experimental Setup and Protocol

A continuous-wave fNIRS brain imager (CW-6, Techen Inc., Milford, Massachusetts) was used to map the ΔHbO and ΔHb induced by sensorimotor cortical activation during a finger-tapping task. As ΔHb dynamics are highly correlated with those of ΔHbO ³² and have significantly lower amplitudes than the latter making them susceptible to cross talk from ΔHbO ³³ and to interference from physiological artifacts, we have focused on the analysis of ΔHbO dynamics only. The source-detector probe geometry of fNIRS is shown in Fig. 1. There were 16 sources and 32 detector fiber bundles to cover most of the sensorimotor cortex. The rows of sources and detectors were centered around the Cz position of the EEG International 10/20 system³⁴ and attached onto the subjects' heads by perforated Velcro straps. Near-infrared light at wavelengths of 690 and 830 nm was delivered from the source fiber bundles simultaneously at each source location as the CW-6 system enables all laser sources to be on at the same time with distinct modulation frequencies (6.4 to 12.6 kHz, with an increment of 200 Hz). The back-reflected light was sampled at the frequency of 25 Hz. Each source had up to six detectors with 3 cm separation, and each detector received light from up to three sources, which resulted in a total of 84 source-detector pairs for each wavelength. This setup enabled monitoring cortical activation over an 11 cm \times 20 cm field of view. Additionally, eight short-distance (1.5 cm) source-detector pairs, indicated by yellow lines in Fig. 1, were used as references to subsequently filter out superficial background hemodynamics unrelated to activation (Sec. 2.3).

EEG International 10/20 system Cz, C3, C4, F3, and F4 anatomical measurements³⁴ were used as reference points to ensure the optical probe setup was placed over the sensorimotor cortex. The optical probe setup was centered on the Cz reference point

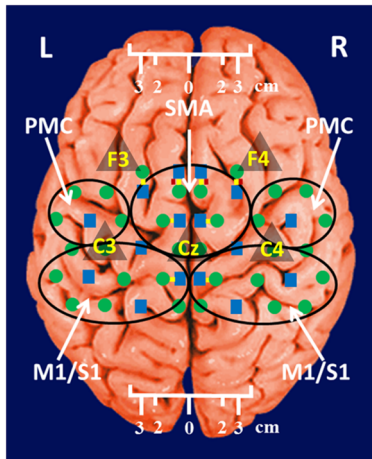


Fig. 1 The fNIRS measurement geometry (sources: blue squares; detectors: green circles) spanned a field of view covering the premotor cortex (PMC), supplementary motor area (SMA) and M1/S1 (primary motor/sensory cortex) areas indicated by black ovals. Yellow lines connect the short distance source-detector pairs sampling the scalp hemodynamics. Dark gray triangles indicate the EEG International 10/20 system Cz, C3, C4, F3, and F4 locations.

and covered a large area of sensorimotor cortex such that the probe set extended a fixed distance of 5 cm anterior to the C3 and C4 positions to map the primary motor/sensory area (M1/S1) and was 0.21 ± 0.13 cm posterior of the measured F3 and F4 positions covering the supplementary motor area (SMA) and premotor cortex (PMC) of both hemispheres, as indicated in Fig. 1. Anatomical measurements were performed on the head of each subject at all three visits and the standard deviations of the distances between Cz and any one of C3, C4, F3, and F4, across all visits, did not exceed $\sim \pm 1.5$ mm.

After subjects were set up for fNIRS measurements they were asked to perform a finger-tapping task, once with their left hand and once with their right hand. Subjects were instructed to tap with four fingers in unison (excluding the thumb) and keep their wrists on the table, while the other hand was to remain at rest as much as possible. An animation made on Adobe flash (Adobe Systems Incorporated, San Jose, California) guided the subjects to tap at a frequency of 1 Hz. The experimental protocol for finger tapping by each hand started with a 3-min rest period, followed by eight 40-s blocks that started with 15 s of tapping followed by 25 s of rest.

2.3 Signal Processing and Image Analysis

In addition to detecting hemodynamic changes due to evoked cortical activation, fNIRS is also sensitive to cerebral hemodynamic fluctuations of systemic origin, which can be caused by cardiac pulsation (0.8–2.0 Hz), respiration (0.1–0.33 Hz) and Mayer waves (0.1 Hz or lower).^{35,36} The cortical hemodynamic response to the motion activation protocol can be found in the frequency range of 0.01–0.4 Hz, so a bandpass filter could only effectively remove cardiac pulsation, but not the respiration or Mayer waves that overlap in frequency with the activation-induced hemodynamic fluctuations. In order to filter out these physiological interferences, recent studies have used component analyses,^{37,38} state-space estimation,^{35,39} adaptive filtering,⁴⁰ linear regression,⁴¹ or some combination of these.^{42,43}

This study used a combination of bandpass filtering, adaptive filtering, and principal component analysis (PCA) to filter the

fNIRS signals as we have previously reported.³¹ In brief, the first step was to use a 0.01–0.4 Hz bandpass filter to remove cardiac pulsation signals. Subsequently, global fluctuations due to respiration and Mayer waves were removed by a combination of an adaptive least-mean-square (LMS) filter⁴⁰ and PCA.³⁷ One short source-detector pair of the eight available was used as the adaptive filter noise reference for the removal of global hemodynamic fluctuations from the fNIRS signals.⁴⁰ The reference channel chosen had the least amount of motion artifacts of the eight, which translated to having either zero or one motion-generated spikes in the time-series reference data. The spike in the reference channel time-series data was manually removed and the missing data were interpolated by the spline cubic spline function in MATLAB® (Mathworks, Natick, Massachusetts). Moreover, any block of data with obvious motion artifacts in any tapping/rest period was manually excluded from further analysis.

Reconstruction and visualization of fNIRS images from the acquired reflectance data were performed by the open-source Homer software implemented in MATLAB.⁴⁴ In this software, activation images were reconstructed by the Tikhonov perturbation solution to the photon diffusion equation, which employs a regularized Moore-Penrose inversion scheme.^{45,46} The resulting ΔHbO maps were reconstructed 20×21 pixel images ($0.55 \text{ cm} \times 0.95 \text{ cm}$ for each pixel) for every 0.04 s time interval.

The determination of image pixels with activation was based on a two-step process. First, the image pixels with temporal hemodynamic patterns that correlated significantly with evoked cortical activation were identified by a general linear model (GLM) similar to previous fMRI studies.^{47–49} A value of $p < 0.0001$ based on Bonferroni's correction was used as the threshold to identify pixels with activation. Second, a k -means clustering algorithm⁵⁰ was used to calculate the signal-to-noise ratio (SNR) per image pixel. This was done to exclude any pixels with low SNR that the GLM still found to significantly correlate with the model-based hemodynamic response function⁵¹ calculated for the finger-tapping protocol being used in this study. The algorithm considered the entire temporal responses for each pixel after GLM and divided the pixel values into three clusters: activation, baseline, or deactivation.³¹ The pixel values in the baseline cluster were regarded as noise. The SNR of activation for each pixel was then calculated as the mean signal amplitude of the activation cluster over the standard deviation of the hemodynamic fluctuation amplitudes of the noise cluster in that pixel. Pixels with $\text{SNR} \geq 2$ were considered to be part of the regions of activation when the ΔHbO amplitude equaled or exceeded two standard deviations of the amplitude of background hemodynamic fluctuations. The selected SNR threshold corresponded to a probability of 95%, or more, for the fluctuation amplitudes of these pixels to be different from those due to background hemodynamics.

The sequence of postprocessing steps described above is shown in Fig. 2. More details can be found in a prior publication from our group.³¹

2.4 fNIRS-Based Metrics Derived from Activation Images and Detector Level Resting-State Data

The laterality index and time-to-peak/duration metrics were derived from the analysis of activation images. The time series data from each subject were first analyzed to find all image pixels with significant activation, as above described in Sec. 2.3.

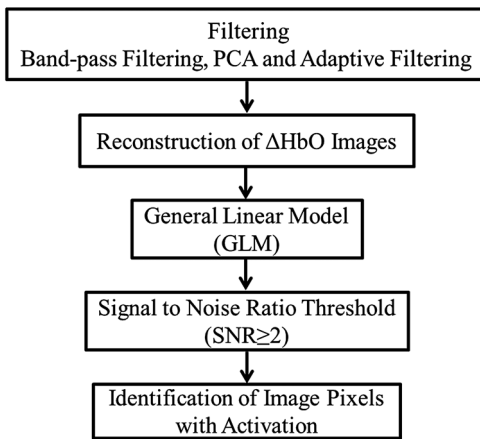


Fig. 2 Flowchart of postprocessing steps.

Subsequently, the laterality index metric was calculated using Eq. (1) and the time-to-peak metric was computed for each pixel with activation and was then averaged across pixels. The resting-state functional connectivity between sensorimotor regions was computed from source-detector channel data that were first averaged within each region indicated in Fig. 1.

2.4.1 Laterality index

Laterality of activation, representing the dominance of one side of the brain in controlling motor functions, was quantified by the laterality index.⁵²

$$L = \frac{N_{\text{contral}} - N_{\text{ipsi}}}{N_{\text{contral}} + N_{\text{ipsi}}}, \quad (1)$$

where N_{contral} was the number of activation pixels in the contralateral hemisphere and N_{ipsi} was the number of activation pixels in the ipsilateral hemisphere. Equation (1) indicates that an L value of “+1” corresponds to complete contralateral activation, an L value of “−1” represents complete ipsilateral activation, and an L of “0” reflects bilateral activation. The midline separating the two hemispheres for calculating laterality index was shifted for Subject 3, as described in Sec. 2.1. The laterality index was averaged across subjects for each visit time point before comparing data between visits.

2.4.2 Resting-state functional connectivity

Resting-state functional connectivity represents the regional interactions between cortical centers that occur when a subject is not performing an explicit task.⁵³ Source-detector channels were assigned to the M1/S1, PMC, or SMA, as identified by the EEG International 10/20 system Cz, C3, C4, F3, and F4 anatomical measurements.²⁸ Signals recorded during the 3-min rest period at the beginning of the protocol were averaged for all detector fiber bundles found within M1/S1, PMC, or SMA and separately for each hemisphere. Due to Subject 3’s anatomical midline shift, as described in Sec. 2.1, only those source and detectors that were at least 2 cm to the right of the measured Cz position were considered part of the right hemisphere. The resting-state functional connectivity between these sensorimotor areas was subsequently computed using a synchronization likelihood (SL) metric.⁵⁴ Cortical regions were considered as functionally connected for $SL \geq 0.6$.⁵⁵ This threshold was lower than

what is typically used in studies on adults,^{56,57} as the correlation strength is known to be weaker in children.⁵⁸ The connection frequency between pairs of sensorimotor regions was calculated for each visit time point as the percentage of subjects having this connection according to the SL metric used.

2.4.3 Activation time-to-peak/duration

Temporal aspects of cortical activation patterns in fNIRS images were quantified by the time-to-peak/duration metric. The rationale behind this metric was that in children with CP, performing finger tapping the time-to-peak tends to be shorter and the activation duration longer compared to controls.³¹ Thus, an increase in this ratio would reflect treatment-induced normalization of activation patterns. The duration of activation in each pixel was defined as the total time for which the hemodynamic fluctuation amplitude in that pixel exceeded a threshold, which was defined as the maximum value of the baseline cluster identified by the *k*-means algorithm (Sec. 2.3). The activation duration metric was then computed as the average of all image pixels within the activation area. The time difference between the beginning of the tapping interval and the time point of maximum ΔHbO , averaged over all pixels with activation in the image, was defined as the time-to-peak metric. Time-to-peak/duration was averaged across subjects for each visit before comparing data between visits.

2.4.4 Statistical analysis

Two-sample *t* tests were performed using SAS 9.2 (SAS Institute Inc. Cary, North Carolina) to determine whether there was a significant difference ($p < 0.05$) of metric means between control subjects and subjects with CP. Paired *t* tests were also performed to determine if there was a significant difference ($p < 0.05$) of metric means between visits of subjects with CP. In the cases where pair-wise dataset comparison did not satisfy the normality condition (function proc univariate normal in SAS, $p < 0.05$), the Wilcoxon signed-rank test was performed instead. Repeated ANOVA tests were performed to check whether there was a significant difference ($p < 0.05$) of metric means between the visits of controls. A posthoc power analysis was performed to validate the statistical power ($1 - \beta$) of the *t* test or Wilcoxon sign-rank test, as appropriate, for the cases where there was a statistically significant difference between the two metric categories being compared.⁵⁹

3 Results

It was found that when children with CP tapped with their unaffected hand, there were no statistically significant changes for any of the fNIRS activation metrics between measurement time points. In this work, the activation metrics obtained from children with CP tapping with their affected hand were compared to those obtained from controls tapping with their dominant hand at the same measurement time points.

3.1 Laterality Index

Activation in M1/S1 cortical regions only was used for the laterality index metric calculations following previously reported fMRI and fNIRS studies.^{16,18,60} Figure 3 shows the mean and standard deviation of the laterality index for controls and children with CP. The three visits for the controls were averaged into a single group of values as the laterality index was not found to

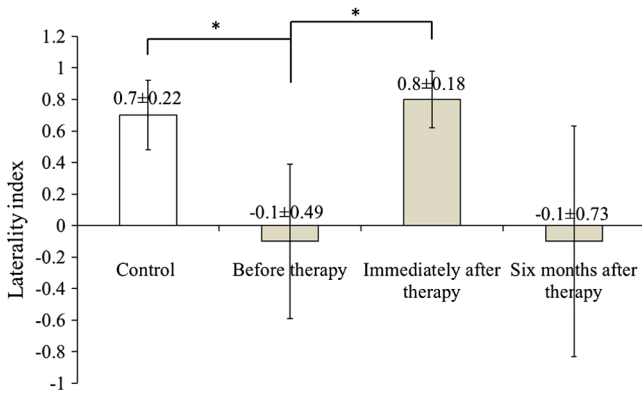


Fig. 3 Laterality index for controls tapping with their dominant hand and children with cerebral palsy (CP) tapping with their affected hand across the three visits (white: controls, gray; children with CP). Error bars indicate \pm one standard deviation. Asterisks indicate statistically significant differences in laterality index ($p < 0.01$).

change significantly over time for these subjects ($p = 0.84$). As shown in Fig. 3, controls had preferential activation in the contralateral sensorimotor cortex during finger tapping. In contrast, children with CP showed bilateral activation on average before therapy. At the second visit immediately after therapy, the laterality index for children with CP increased and was closer to that of controls. At 6 months after therapy only one child with CP retained a high laterality index while all others relapsed. As a result, the mean laterality index relapsed close to the values before treatment.

A high statistical significance was found ($p = 0.007$, $1 - \beta = 0.91$) for the mean value difference in laterality

index between controls and children with CP before therapy. Moreover, the laterality index of children with CP immediately after therapy was significantly different ($p = 0.006$, $1 - \beta = 0.98$) from that of before therapy. No significant difference was observed between 6 months after therapy and prior visits due to the larger standard deviation of the group's laterality index 6 months after therapy.

3.2 Resting-State Functional Connectivity

Changes in the resting-state functional connectivity between five cortical regions (Fig. 1) were explored as a metric of response to CIMT. Based on the aforementioned $SL \geq 0.6$ criterion, the two MACS 1 subjects showed significant pair-wise connectivity between all sensorimotor regions that did not change between the three visits. The four children with CP that did not show connectivity changes, all MACS 2, were compared to the average connectivity pattern from five controls in this part of the study. The thickness of lines in Fig. 4 connecting any two sensorimotor regions represents the percentage of MACS 2 subjects for whom a given pair of activation regions was connected.

The frequency of connections between any two regions for controls was no more than 60%. In contrast, the frequency of pair-wise connection between regions for MACS 2 subjects before therapy was much higher, even reaching 100% for some connections between the SMA and other cortical regions. Interestingly, immediately after therapy MACS 2 subjects had weaker connectivity frequencies, especially between the SMA and other cortical regions, which was similar to what was observed in controls. Therefore, these results imply a certain

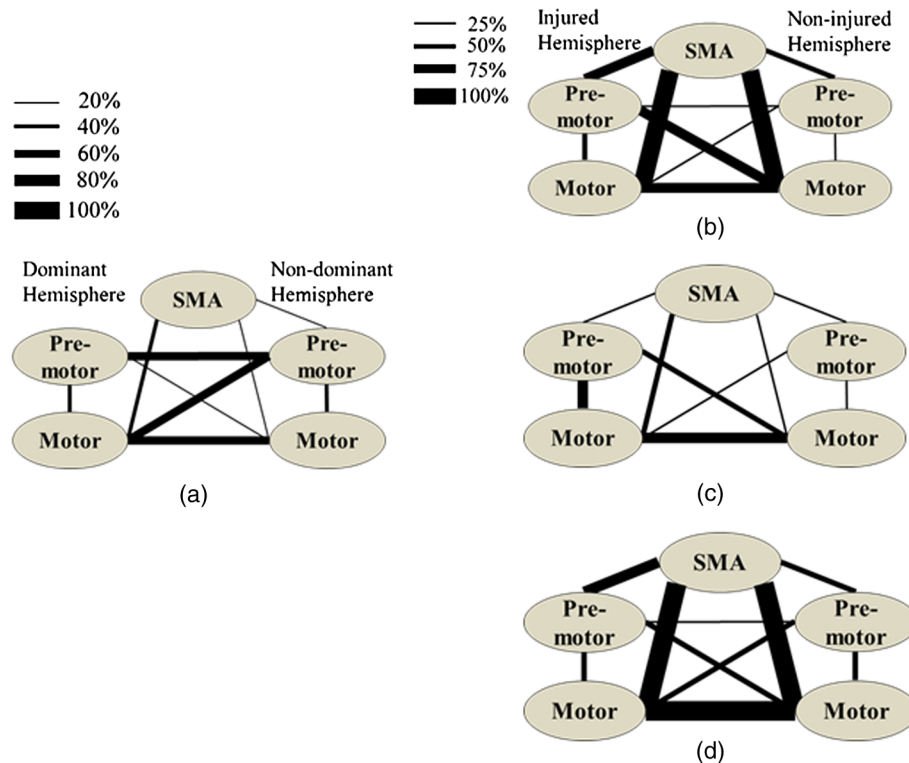


Fig. 4 Group-wise resting-state functional connectivity in controls (a) and children with CP at the three assessment time points: (b) before therapy, (c) immediately after therapy, (d) 6 months later after therapy. Black line thickness represents the percentage of subjects with significant connectivity between a given pair of sensorimotor centers.

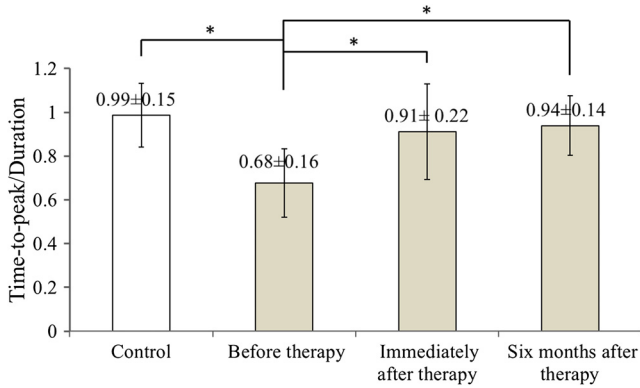


Fig. 5 Time-to-peak/duration of activation for controls tapping with their dominant hand and children with CP tapping with their affected hand across the three visits (white: controls; gray: children with CP). Error bars indicate \pm one standard deviation. Asterisks indicate statistically significant differences in time-to-peak/duration ($p < 0.05$).

level of sensorimotor network normalization occurring immediately after CIMT. However, at the 6 months after therapy time point, the connectivity frequencies between almost all cortical regions reversed back toward values found before therapy.

3.3 Activation Time-to-Peak/Duration

Figure 5 shows the mean and standard deviation of the time-to-peak/duration metric for controls and the three visits of children with CP. As was done for the laterality index analyses above, all pair-wise group comparisons between visits of children with CP for the time-to-peak/duration metric were performed by paired t tests with one exception: The comparison of children with CP before therapy versus immediately after therapy. This latter case did not pass the normality test (Sec. 2.4.4) and the Wilcoxon signed-rank test was used instead. No significant difference was observed for controls between the three visits ($p = 0.69$) and they were averaged into a single group. A significant difference was found in time-to-peak/duration between controls and children with CP before therapy ($p = 0.001$, $1 - \beta = 0.97$). Most subjects with CP had a smaller time-to-peak/duration metric before therapy, which increased significantly immediately after therapy ($p = 0.03$, $1 - \beta = 0.99$) and persisted at significantly higher values ($p = 0.006$, $1 - \beta = 0.97$) 6 months after

therapy. The change of time-to-peak/duration toward higher values indicates a normalization of temporal activation patterns in all five sensorimotor regions after CIMT that persisted even 6 months later.

3.4 Comparisons with Clinical Assessment Scores

3.4.1 Changes in Melbourne and AHA scores between visits

The Melbourne and AHA scales were employed to evaluate the unimanual and bimanual performance, respectively, of children with CP before, immediately and 6 months after therapy. Figure 6 illustrates changes in Melbourne scores versus changes in AHA scores for children with CP between visits. The thresholds for clinically significant improvements in Melbourne and AHA scores were 14 and 5, respectively.^{12,13} These threshold values are depicted in Fig. 6 as dashed lines.

Changes in clinical scale scores varied greatly between immediately after therapy [Fig. 6(a)] and 6 months after therapy [Fig. 6(b)]. Nevertheless, all four MACS2 subjects improved significantly on Melbourne or AHA scores, or both, immediately after therapy and 6 months after therapy. On the contrary, the two MACS 1 subjects included in this study, Subjects 1 and 4 [circled with black ovals in Figs. 6(a) and 6(b)], did not show significant improvements on either assessment scale. As a result, the discussion below on the comparisons between clinical scale scores and fNIRS metrics focuses on the four MACS 2 subjects, who had significant changes in motor function after CIMT.

3.4.2 Changes in Melbourne and AHA scores versus changes in laterality index

Figures 7(a) and 7(b) illustrate the comparison between the change in Melbourne scores and the change in laterality index between visits for the four MACS 2 subjects. It is seen that for all subjects except for Subject 3, an increase in the laterality index representing a shift of cortical activation from the ipsilateral to the contralateral hemisphere was accompanied by significant improvements in unimanual ability immediately after therapy, as reflected by the increased Melbourne scores [Fig. 7(a)]. The fact that Subject 3 appears to be an outlier is not surprising given that he had previously had brain surgery due to intractable epileptic seizures (Sec. 2.1). The laterality

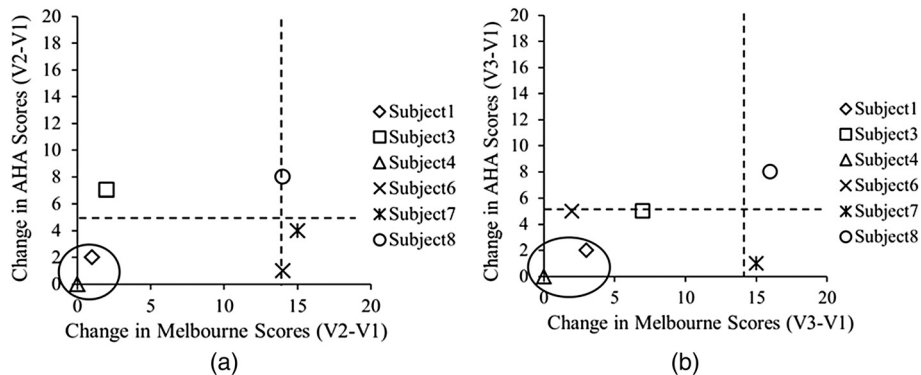


Fig. 6 Change in clinical scores for six subjects with CP between visits (V1: before therapy, V2: immediately after therapy, V3: 6 months after therapy). (a) Change in scores between before and immediately after therapy (V2-V1). (b) Change in scores between before and 6 months after therapy (V3-V1). Thresholds for clinically significant improvements in Melbourne and AHA scores were 14 (vertical dashed lines) and 5 (horizontal dashed lines), respectively. Data for MACS1 subjects are inside ovals.

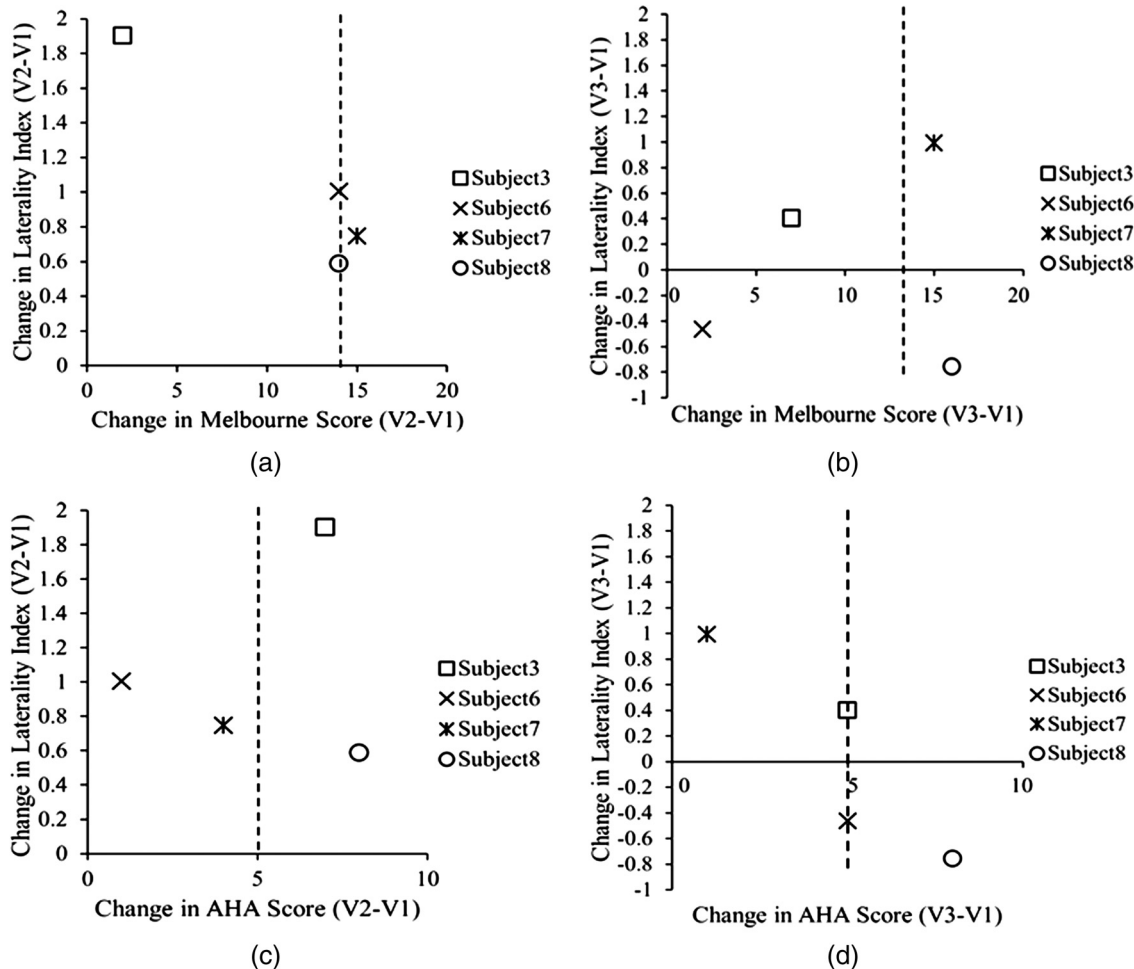


Fig. 7 Change in clinical scores versus change in laterality index for MACS 2 subjects between visits (V1: before therapy, V2: immediately after therapy, V3: 6 months later after therapy). Change in Melbourne scores versus change in laterality index immediately after therapy (a) and (b) 6 months after therapy. Corresponding changes in AHA scores immediately after therapy (c) and (d) 6 months after therapy.

index change of 2 for this subject indicates a complete switch of activation between hemispheres toward a more normal laterality pattern that, however, did not result in significant motor gains [Fig. 7(a)]. At 6 months after CIMT [Fig. 7(b)] Subject 6 had relapsed but all other subjects maintained and even slightly improved unimanual ability compared to before therapy. Even though there are not enough subjects to perform formal statistical analyses, one can see a positive trend between the laterality index and Melbourne score changes in Fig. 7(b).

In contrast to Melbourne score changes, an overall negative trend between laterality index and AHA score changes could be discerned both immediately after therapy [Fig. 7(c)] and 6 months after therapy [Fig. 7(d)]. An exception to this trend was Subject 8 who had improvements in both Melbourne and AHA scores that were maintained 6 months later, but at the cost of a significant relapse in laterality index 6 months after therapy that was even more abnormal than the values before therapy.

Another noteworthy observation was that Subject 7 was the only one in the MACS 2 group who retained significant improvements in unilateral motor function, as assessed by the Melbourne scale, while also maintaining a normalized

laterality index [Fig. 7(b)]. Interestingly, Subject 7 also had the highest average connectivity strength between sensorimotor centers ($SL = 0.70$) compared to the MACS2 group average ($SL = 0.64$). Nevertheless, the connectivity pattern for Subject 7 was not different from that of the group average shown in Fig. 4(d).

Overall, the above results showed that each child had a unique way of responding to CIMT and attained some motor function improvements by increasing the involvement of the ipsilateral sensorimotor cortex (Subject 8), increasing the connectivity strength between sensorimotor centers (Subject 7), or by some combination thereof (Subjects 3 and 6). A positive trend between increases in Melbourne scores and increases in time-to-peak/duration, as well as a negative trend between increases in AHA scores and increases in time-to-peak/duration were also noticed. All results are compiled in Table 1.

4 Discussion

For unilateral brain lesions causing hemiplegia, there is a natural tendency for the affected sensorimotor control areas to recruit corresponding areas from the contralateral unaffected cerebral hemisphere. The increased connectivity between hemispheres

Table 1 Clinical scores and functional near-infrared spectroscopy (fNIRS) metrics of subjects with cerebral palsy (CP) and controls before, immediately after and 6 months after therapy (V1: before therapy, V2: immediately after therapy, V3: 6 months after therapy).

Subject	Clinical scores						fNIRS metrics					
	Melbourne			AHA			Laterality index			Time-to-peak/duration		
	V1	V2	V3	V1	V2	V3	V1	V2	V3	V1	V2	V3
S1	110	111	113	60	62	62	0.5	1	0.4	0.92	1.15	1.13
S3	74	76	81	34	41	39	-1	0.9	-0.6	0.62	0.81	0.86
S4	117	117	117	84	84	84	0	1	—	0.80	1.22	—
S6	45	59	47	47	48	52	0.1	0.9	-0.6	0.62	0.85	0.81
S7	54	69	69	64	68	65	-0.1	0.6	0.9	0.52	0.73	0.86
S8	58	72	74	44	52	52	0	0.6	-0.8	0.56	0.71	1.04
Controls (Averaged)	—	—	—	—	—	—	0.69	0.71	0.69	0.97	0.99	1.00

is presumed to be a compensatory reaction to the loss of connections with white matter after brain injury.⁶¹ CIMT has been used to enforce increased use of the affected hand and reduce overreliance on the unaffected hemisphere,⁸ which is accompanied by partial normalization of brain activation patterns.^{16,18}

In this work, fNIRS was used to map the plastic changes that occurred in the sensorimotor cortex of six children with CP immediately after and 6 months after 2 weeks of CIMT. Changes in the unimanual and bimanual abilities of these children were assessed by the Melbourne and AHA functional scales, respectively, at the same time points as fNIRS measurements. Subsequent data analysis and comparisons yielded some interesting insights:

First, though larger numbers of subjects would need to be tested in the future, the improvements in clinical scores reported in this work for MACS 2 subjects suggest that children with CP with a higher level of motor impairment could benefit more from CIMT, consistent with findings from a prior clinical report.⁶² The two less impaired MACS 1 subjects did not benefit as much, as proven by the nonsignificant changes in their clinical scores after CIMT (Fig. 6). These subjects had high manual ability scores to begin with. As this was an initial exploratory study, only children with CP with a lower level motor impairment classified as MACS 1 or MACS 2 were included to avoid possible issues with more impaired subjects who may have had difficulty following the fNIRS finger-tapping protocol.

Second, there were no children with CP in this study that significantly improved both their unimanual and bimanual abilities after CIMT while also normalizing their sensorimotor activation patterns, as measured by fNIRS. Normalization in this context meant that the laterality index and time-to-peak/duration metric values became closer to corresponding values seen in the group of healthy children that were closer to unity for both metrics. From Figs. 6(a) and 6(b), it was interesting to see that for three of the four MACS 2 subjects (Subjects 3, 6, and 7) there was significant improvement in either the Melbourne or AHA scores, but not both, at any one assessment time point. Since Melbourne scores reflected unimanual ability and AHA scores reflected bimanual ability, it is possible that a trade-off existed between using unilateral or compensatory bilateral limb movements to perform manual tasks. This trade-off was also observed

by the positive trend between laterality index and Melbourne score changes in Fig. 7(b) and an overall negative trend between laterality index and AHA score changes both immediately after therapy [Fig. 7(c)] and 6 months after therapy [Fig. 7(d)]. This observation suggests that normalization of the laterality index, while improving unimanual ability [Fig. 7(b)], results in the trade-off of reduced bimanual ability [Fig. 7(d)] for these children. However, one MACS 2 subject, Subject 8, had significant improvements immediately after therapy that persisted 6 months after therapy for both clinical assessment scales. This subject not only improved the use of the affected arm, but also the cooperation between arms. However, the negative change in laterality index for this subject at 6 months after CIMT [Fig. 7(b)] suggests that the improvement in Melbourne score (unimanual ability) occurred at the expense of abnormally high compensatory use of the uninjured brain hemisphere.

Third, an interesting difference was observed between how the time-to-peak/duration changed with time post-therapy compared to the laterality index and resting-state connectivity metrics studied here: Time-to-peak/duration, a local measure of hemodynamic response, sustained the improvements seen immediately after CIMT out to 6 months after therapy. In contrast, laterality index and resting-state connectivity, which are global measures of hemodynamic response, normalized immediately after CIMT but relapsed 6 months after therapy toward the values before therapy. These observations suggest that the global metrics of hemodynamic pattern change may be more useful than local metrics for assessing longer term treatment response.

The results of this work are consistent with results from the few fMRI studies that exist to date on the topic of CP and CIMT.^{16,18} Specifically, in a case report on a child with CP with MACS2, the laterality index changed from -0.25 before 3 weeks of CIMT to 0.43 immediately afterward.¹⁶ In another study, including four children with CP (MACS1 and MACS2), two maintained a high laterality index between before (0.80 ± 0.08) and immediately after CIMT (0.72 ± 0.07) while the other two showed a positive shift in laterality index from -0.14 ± 0.16 before to 0.34 ± 0.13 after CIMT.¹⁸ In all, in these prior studies, subjects with a low pre-CIMT laterality index showed an increase immediately after therapy.

These studies also reported concurrent improvements in manual ability metrics after CIMT, but the limited number of subjects studied and the variability of manual ability assessment methods used between studies precludes any further comparisons. Finally, an fMRI resting-connectivity study on children with CP showed similar bilateral patterns as reported in this work,⁶³ but the effects of CIMT on resting-connectivity patterns have not been previously reported.

5 Conclusion

This work demonstrated the utility of portable fNIRS technology as a means of mapping sensorimotor cortex plasticity in children with CP to help explain changes seen in manual ability after a therapeutic intervention. The fNIRS results provided insights that would not be accessible by looking at changes in clinical scores alone. Larger numbers of subjects would need to be followed in future studies for longer periods of time to assess whether fNIRS metrics could be used as predictors of CIMT outcomes.

Acknowledgments

Support for this work was provided in part by the National Institute of Biomedical Imaging and Bioengineering (NIBIB), Grant No. 1R01EB013313-01.

References

- P. Rosenbaum et al., "A report: the definition and classification of cerebral palsy April 2006," *Dev. Med. Child Neurol. Suppl.* **109**(suppl 109), 8–14 (2007).
- W. Kulak et al., "Neurophysiologic and neuroimaging studies of brain plasticity in children with spastic cerebral palsy," *Exp. Neurol.* **198**(1), 4–11 (2006).
- J. M. Keogh and N. Badawi, "The origins of cerebral palsy," *Curr. Opin. Neurol.* **19**(2), 129–134 (2006).
- A. Houwink et al., "A neurocognitive perspective on developmental disregard in children with hemiplegic cerebral palsy," *Res. Dev. Disabil.* **32**(6), 2157–2163 (2011).
- A. Van de Winkel et al., "How does brain activation differ in children with unilateral cerebral palsy compared to typically developing children, during active and passive movements, and tactile stimulation? An fMRI study," *Res. Dev. Disabil.* **34**(1), 183–197 (2013).
- R. Boyd et al., "Management of upper limb dysfunction in children with cerebral palsy: a systematic review," *European J. Neurol.* **8**(s5), 150–166 (2001).
- J. Charles and A. M. Gordon, "A critical review of constraint-induced movement therapy and forced use in children with hemiplegia," *Neural Plast.* **12**(2–3), 245–261 (2005).
- B. Hoare et al., "Constraint-induced movement therapy in the treatment of the upper limb in children with hemiplegic cerebral palsy," *Clin. Rehabil.* **21**(8), 675–685 (2007).
- A. C. Eliasson et al., "The manual ability classification system (MACS) for children with cerebral palsy: scale development and evidence of validity and reliability," *Dev. Med. Child Neurol.* **48**(7), 549–554 (2006).
- M. Law et al., "The Canadian occupational performance measure: an outcome measure for occupational therapy," *Canadian J. Occup. Ther.* **57**(2), 82–87 (1990).
- S. Blundell et al., "Functional strength training in cerebral palsy: a pilot study of a group circuit training class for children aged 4–8 years," *Clin. Rehabil.* **17**(1), 48–57 (2003).
- M. Randall et al., "Reliability of the Melbourne assessment of unilateral upper limb function," *Dev. Med. Child Neurol.* **43**(11), 761–767 (2001).
- L. Krumlinde-sundholm and A.-C. Eliasson, "Development of the assisting hand assessment: a Rasch-built measure intended for children with unilateral upper limb impairments," *Scandinavian J. Occup. Ther.* **10**(1), 16–26 (2003).
- B. S. Russman and S. Ashwal, "Evaluation of the child with cerebral palsy," *Semin. Pediatr. Neurol.* **11**(1), 47–57 (2004).
- K. Himmelmann and P. Uvebrant, "Function and neuroimaging in cerebral palsy: a population-based study," *Dev. Med. Child Neurol.* **53**(6), 516–521 (2011).
- T. L. Sutcliffe et al., "Cortical reorganization after modified constraint-induced movement therapy in pediatric hemiplegic cerebral palsy," *J. Child Neurol.* **22**(11), 1281–1287 (2007).
- C. Sterling et al., "Structural neuroplastic change after constraint-induced movement therapy in children with cerebral palsy," *Pediatrics* **131**(5), e1664–e1669 (2013).
- T. L. Sutcliffe et al., "Pediatric constraint-induced movement therapy is associated with increased contralateral cortical activity on functional magnetic resonance imaging," *J. Child Neurol.* **24**(10), 1230–1235 (2009).
- M. Wilke et al., "Functional magnetic resonance imaging in pediatrics," *Neuropediatrics* **34**(5), 225 (2003).
- H. Juenger et al., "Two types of exercise-induced neuroplasticity in congenital hemiparesis: a transcranial magnetic stimulation, functional MRI, and magnetoencephalography study," *Dev. Med. Child Neurol.* **55**(10), 941–951 (2013).
- F. Irani et al., "Functional near infrared spectroscopy (fNIRS): an emerging neuroimaging technology with important applications for the study of brain disorders," *Clini. Neuropsychol.* **21**(1), 9–37 (2007).
- S. Cutini et al., "Review: functional near infrared optical imaging in cognitive neuroscience: an introductory review," *J. Near Infrared Spectrosc.* **20**(1), 75–92 (2012).
- M. A. Franceschini et al., "Hemodynamic evoked response of the sensorimotor cortex measured noninvasively with near-infrared optical imaging," *Psychophysiology* **40**(4), 548–560 (2003).
- F. Orihuela-Espina et al., "Quality control and assurance in functional near infrared spectroscopy (fNIRS) experimentation," *Phys. Med. Biol.* **55**(13), 3701 (2010).
- V. Toronov et al., "Near-infrared study of fluctuations in cerebral hemodynamics during rest and motor stimulation: temporal analysis and spatial mapping," *Med. Phys.* **27**(4), 801–815 (2000).
- S. C. Bunce et al., "Functional near-infrared spectroscopy," *IEEE Eng. Med. Biol. Mag.* **25**(4), 54–62 (2006).
- K. Takahashi et al., "Activation of the visual cortex imaged by 24-channel near-infrared spectroscopy," *J. Biomed. Opt.* **5**(1), 93–96 (2000).
- M. Ferrari and V. Quaresima, "A brief review on the history of human functional near-infrared spectroscopy (fNIRS) development and fields of application," *Neuroimage* **63**(2), 921–935 (2012).
- U. Chaudhary et al., "Motor response investigation in individuals with cerebral palsy using near infrared spectroscopy: pilot study," *Appl. Opt.* **53**(3), 503–510 (2014).
- M. J. Kurz et al., "An fNIRS exploratory investigation of the cortical activity during gait in children with spastic diplegic cerebral palsy," *Brain Dev.* **36**(10), 870–877 (2014).
- B. Khan et al., "Identification of abnormal motor cortex activation patterns in children with cerebral palsy by functional near-infrared spectroscopy," *J. Biomed. Opt.* **15**(3), 036008 (2010).
- T. Huppert et al., "A temporal comparison of BOLD, ASL, and NIRS hemodynamic responses to motor stimuli in adult humans," *Neuroimage* **29**(2), 368–382 (2006).
- G. Strangman et al., "Factors affecting the accuracy of near-infrared spectroscopy concentration calculations for focal changes in oxygenation parameters," *Neuroimage* **18**(4), 865–879 (2003).
- G. H. Klem et al., "The ten-twenty electrode system of the international federation," *Electroencephalogr. Clin. Neurophysiol. Suppl.* **52**, 3–6 (1999).
- M. A. Franceschini et al., "Diffuse optical imaging of the whole head," *J. Biomed. Opt.* **11**(5), 054007 (2006).
- C. Julien, "The enigma of Mayer waves: facts and models," *Cardiovasc. Res.* **70**(1), 12–21 (2006).
- Y. Zhang et al., "Eigenvector-based spatial filtering for reduction of physiological interference in diffuse optical imaging," *J. Biomed. Opt.* **10**(1), 011014 (2005).
- G. Morren et al., "Detection of fast neuronal signals in the motor cortex from functional near infrared spectroscopy measurements using independent component analysis," *Med. Biol. Eng. Comput.* **42**(1), 92–99 (2004).
- S. Prince et al., "Time-series estimation of biological factors in optical diffusion tomography," *Phys. Med. Biol.* **48**(11), 1491 (2003).

40. Q. Zhang et al., "Adaptive filtering for global interference cancellation and real-time recovery of evoked brain activity: a Monte Carlo simulation study," *J. Biomed. Opt.* **12**(4), 044014 (2007).
41. N. M. Gregg et al., "Brain specificity of diffuse optical imaging: improvements from superficial signal regression and tomography," *Front. Neuroenerg.* **2**(14), 1–8 (2010).
42. T. Funane et al., "Quantitative evaluation of deep and shallow tissue layers' contribution to fNIRS signal using multi-distance optodes and independent component analysis," *Neuroimage* **85**(1), 150–165 (2014).
43. L. Gagnon et al., "Improved recovery of the hemodynamic response in diffuse optical imaging using short optode separations and state-space modeling," *Neuroimage* **56**(3), 1362–1371 (2011).
44. T. J. Huppert et al., "HomER: a review of time-series analysis methods for near-infrared spectroscopy of the brain," *Appl. Opt.* **48**(10), D280–D298 (2009).
45. M. E. Kilmer et al., "A projection-based approach to general-form Tikhonov regularization," *SIAM J. Sci. Comput.* **29**(1), 315–330 (2007).
46. J. Wang, "Recurrent neural networks for computing pseudoinverses of rank-deficient matrices," *SIAM J. Sci. Comput.* **18**(5), 1479–1493 (1997).
47. K. J. Friston et al., "Statistical parametric maps in functional imaging: a general linear approach," *Hum. Brain Mapp.* **2**(4), 189–210 (1994).
48. C. F. Beckmann et al., "General multilevel linear modeling for group analysis in fMRI," *Neuroimage* **20**(2), 1052–1063 (2003).
49. A. F. Abdelnour and T. Huppert, "Real-time imaging of human brain function by near-infrared spectroscopy using an adaptive general linear model," *Neuroimage* **46**(1), 133–143 (2009).
50. J. MacQueen, "Some methods for classification and analysis of multivariate observations," in *Proc. Fifth Berkeley Symp. on Mathematical Statistics and Probability*, pp. 281–297, California (1967).
51. M. A. Lindquist et al., "Modeling the hemodynamic response function in fMRI: efficiency, bias and mis-modeling," *Neuroimage* **45**(1 Suppl), S187–S198 (2009).
52. M. L. Seghier, "Laterality index in functional MRI: methodological issues," *Magn. Reson. Imaging* **26**(5), 594–601 (2008).
53. B. B. Biswal, "Resting state fMRI: a personal history," *Neuroimage* **62**(2), 938–944 (2012).
54. B. Khan et al., "Functional near-infrared spectroscopy maps cortical plasticity underlying altered motor performance induced by transcranial direct current stimulation," *J. Biomed. Opt.* **18**(11), 116003 (2013).
55. D. Tomasi and N. D. Volkow, "Abnormal functional connectivity in children with attention-deficit/hyperactivity disorder," *Biol. Psych.* **71**(5), 443–450 (2012).
56. E. J. Sanz-Arigita et al., "Loss of 'small-world' networks in Alzheimer's disease: graph analysis of fMRI resting-state functional connectivity," *PLoS One* **5**(11), e13788 (2010).
57. R. C. Mesquita et al., "Resting state functional connectivity of the whole head with near-infrared spectroscopy," *Biomed. Opt. Express* **1**(1), 324–336 (2010).
58. D. A. Fair et al., "The maturing architecture of the brain's default network," *Proc. Natl. Acad. Sci.* **105**(10), 4028–4032 (2008).
59. F. Faul et al., "G* Power 3: a flexible statistical power analysis program for the social, behavioral, and biomedical sciences," *Behav. Res. Methods* **39**(2), 175–191 (2007).
60. F. Tian et al., "Quantification of functional near infrared spectroscopy to assess cortical reorganization in children with cerebral palsy," *Opt. Express* **18**(25), 25973–25986 (2010).
61. H. Burton et al., "Functional connectivity for somatosensory and motor cortex in spastic diplegia," *Somatosens. Motor Res.* **26**(4), 90–104 (2009).
62. L. Sakzewski et al., "Best responders after intensive upper-limb training for children with unilateral cerebral palsy," *Arch. Phys. Med. Rehabil.* **92**(4), 578–584 (2011).
63. C. Papadelis et al., "Cortical somatosensory reorganization in children with spastic cerebral palsy: a multimodal neuroimaging study," *Front. Hum. Neurosci.* **8**(725), 1–15 (2014).

Jianwei Cao received her BS and MS degrees in optical engineering from Hefei University of Technology, Hefei, China, in 2008 and 2011, respectively. Currently, she is working toward her PhD with George Alexandrakis's group in bioengineering at the University of Texas at

Arlington, Texas. Her research mainly focuses on functional near infrared spectroscopy, brain imaging, and biomedical signal processing.

Bilal Khan received his BS degree in electrical engineering from the University of Texas at Austin in 2007. He completed his MS degree in 2009 and then completed his doctoral studies in 2014 in biomedical engineering from the joint program of biomedical engineering at the University of Texas at Arlington and the University of Texas Southwestern Medical Center at Dallas. His research focus has been in signal processing, bioinstrumentation, and optical imaging.

Nathan Hervey earned his BS degree in mechanical engineering from Texas A&M University in May of 2009. In the fall of 2011, he began his studies in bioengineering at the University of Texas at Arlington with Dr. George Alexandrakis as his adviser. His research focused on new analysis techniques for functional near-infrared spectroscopy data.

Fenghua Tian is a faculty associate researcher at the University of Texas at Arlington, Arlington, Texas. He received his doctoral degree from Tsinghua University, Beijing, China. His major research interests focus on functional near-infrared spectroscopy and diffuse optical tomography, brain imaging, and biomedical signal processing.

Mauricio R. Delgado is the director of pediatric neurology at Texas Scottish Rite Hospital for Children and professor of neurology and neurotherapeutics at the University of Texas Southwestern Medical Center at Dallas. He received his MD degree from the University of Monterrey and did his residency in pediatrics and neurology at the University of Ottawa. He is board certified in neurology. He specializes in neurorehabilitation of children with motor disorders of central origin and neurogenetic disorders.

Nancy J. Clegg is the childhood motor disorders research coordinator at Texas Scottish Rite Hospital for Children in Dallas, Texas. She received her BSN from Vanderbilt University in Nashville, Tennessee, her MSN from the University of Texas Health Science Center in San Antonio, Texas, and her PhD from the University of Texas at Austin. She is an advanced practice nurse and is a certified clinical research professional by the Society of Clinical Research Associates.

Linsley Smith is a research coordinator at Texas Scottish Rite Hospital for Children in Dallas, Texas. She received her BSN from the University of Texas at Austin and is also a certified clinical research professional by the Society of Clinical Research Associates.

Heather Roberts is an occupational therapist at Texas Scottish Rite Hospital for Children in Dallas, Texas. She received her BS degree in occupational therapy from Saint Louis University in St. Louis, Missouri, and her master's degree in healthcare administration from the University of Texas at Arlington, Texas.

Kirsten Tulchin-Francis is the director of Movement Science Laboratory at Texas Scottish Rite Hospital for Children and serves as an assistant professor for the Prosthetics and Orthotics Program in the School of Health Professions at the University of Texas Southwestern Medical Center at Dallas. She received her PhD in kinesiology-biomechanics from Texas Woman's University. Her research interests include foot and ankle biomechanics and functional outcomes in hip pathology, lower limb deficiencies, and scoliosis.

Angela Shierk is an occupational therapist at Texas Scottish Rite Hospital for Children in Dallas, Texas. She received her master's degree in occupational therapy from Texas Tech University Health Sciences Center in Lubbock, Texas, and her PhD from Texas Woman's University in Denton, Texas. She is a practicing occupational therapist and an adjunct faculty member in the Occupational Therapy Department at Texas Woman's University in Denton, Texas.

Laura Shagman received her BS and MS degrees in electrical engineering in 2007 and 2009, respectively, from the University of Texas at Dallas. Afterward, she was hired as a technical sales associate and is currently a technical sales representative for Texas Instruments.

Duncan MacFarlane is a professor of electrical engineering at UT Dallas. He received his BSEE and MSEE degrees from Brown University and his PhD from Portland State University. He has worked at Schafer Associates, Texas Instruments, and at JDS Uniphase, Celion Networks and was a co-founder of MRRRA. He teaches courses in electromagnetics and communication systems. He is a registered professional engineer in the state of Texas and a fellow of the Optical Society of America.

Hanli Liu is a full professor of bioengineering at the University of Texas at Arlington. She received her MS and PhD degrees from Wake Forest University in physics, followed by postdoctoral training at the University of Pennsylvania in tissue optics. Her current

expertise lies in the field of near-infrared spectroscopy of tissues, optical sensing for cancer detection, and diffuse optical tomography for functional brain imaging, all of which are related to clinical applications.

George Alexandrakis did his undergraduate studies in physics at Oxford University, UK, and his graduate studies in medical physics at McMaster University, Canada. He was a postdoctoral fellow at Massachusetts General Hospital/Harvard Medical School and at UCLA. As faculty at the University of Texas at Arlington's Bioengineering Department since 2006, his research has focused on the development of novel optical imaging methods for biomedical applications.